Published in final edited form as:
Polymer (Guildf). 2009 December 10; 50(26): 6331–6339. doi:10.1016/j.polymer.2009.05.034.

Hindered Diffusion of Oligosaccharides in High Strength Poly (ethylene glycol)/Poly(acrylic acid) Interpenetrating Network Hydrogels: Hydrodynamic Versus Obstruction Models

Dale J. Waters and **Curtis W. Frank***
Department of Chemical Engineering, Stanford University, 381 North-South Mall, Stauffer III, Stanford, CA 94305-5025, United States

Abstract

Diffusion coefficients of small oligosaccharides within high strength poly(ethylene glycol)/poly (acrylic acid) interpenetrating network (PEG/PAA IPN) hydrogels were measured by diffusion through hydrogel slabs. The ability of hindered diffusion models previously presented in the literature to fit the experimental data is examined. A model based solely on effects due to hydrodynamics is compared to a model based solely on solute obstruction. To examine the effect of polymer volume fraction on the observed diffusion coefficients, the equilibrium volume fraction of polymer in PEG/PAA IPNs was systematically varied by changing the initial PEG polymer concentration in hydrogel precursor solutions from 20 to 50 wt./wt.%. To examine the effect of solute radius on the observed diffusion coefficients, solute radii were varied from 3.3 to 5.1 Å by measuring diffusion coefficients of glucose, a monosaccharide; maltose, a disaccharide; and maltotriose, a trisaccharide. Both the hydrodynamic and obstruction models rely on scaling relationships to predict diffusion coefficients. The proper scaling relationship for each of the hindered diffusion models is evaluated based on fits to experimental data. The scaling relationship employed is found to have a greater significance for the hydrodynamic model than the obstruction model. Regardless of the scaling relationship employed, the obstruction model provides a better fit to our experimental data than the hydrodynamic model.

Keywords

hydrogel; diffusion; interpenetrating polymer network

1. Introduction

Hydrogels are crosslinked networks of water-soluble polymers that swell in the presence of water, yet cannot fully dissociate due to the presence of network crosslinks. Hydrogels have recently gained considerable attention primarily for their potential use as drug carriers in drug delivery applications and as cell scaffolds in tissue engineering applications. Recent efforts have focused on synthesizing hydrogels with various functional groups and molecular-level architectures to create gels that exhibit swelling responses to a number of environmental factors

*Corresponding author. Tel: +1 650 723 4573; fax: +1 650 723 9780. Curt.Frank@stanford.edu.

such as temperature, ionic strength, and pH [1,2]. Many of these hydrogel designs are intended to facilitate drug delivery through either polymer degradation to release drug slowly or through hydrogel swelling responses to environmental conditions for rapid and targeted drug release. Although there have been significant efforts to control the release of small molecule and protein-based drugs from hydrogels through various mechanisms, the rate at which these solute molecules simply diffuse through a hydrogel or polymer network will always be an important consideration. For any application that requires drug release or solute transport through a hydrogel, a fundamental understanding of the important factors governing hindered solute diffusion through networks of polymer chains is essential.

The poor mechanical strength of most hydrogels severely limits their use to applications where little or no mechanical strength is required. Recently, Gong et al. demonstrated that hydrogels prepared from interpenetrating polymer networks (IPNs) have dramatically enhanced mechanical properties compared to single networks of each component [3]. Hydrogels with enhanced mechanical strength open the door to a wider variety of applications that require robust mechanical properties, such as synthetic substitutes to load-bearing soft tissues. Our research group is currently developing IPN hydrogels consisting of a poly(ethylene glycol) (PEG) network interpenetrated with a poly(acrylic acid) (PAA) network for use in artificial cornea, corneal inlay, and corneal onlay applications [4-7]. The optical clarity and high mechanical strength of these hydrogels makes them ideal materials for such ophthalmic applications. In addition to optical clarity and mechanical strength, inter-corneal implants must also have a high rate of small molecule nutrient diffusion in order to sustain a viable layer of epithelial cells on the outermost surface of the eye. In order to tune a hydrogel's transport properties to have a sufficiently high diffusivity, an understanding of the critical parameters governing solute diffusion in hydrogels and how these parameters influence diffusion is necessary.

In this study, the diffusivities of a series of oligosaccharides in PEG/PAA IPN hydrogels are compared to the diffusivities predicted by hindered diffusion models previously reported in the literature to determine if these models are applicable to our system. We have measured the diffusion rates of glucose, a monosaccharide; maltose, a disaccharide; and maltotriose, a trisaccharide, through PEG/PAA IPN hydrogels that have varying equilibrium volume fractions of polymer. The polymer content was varied by changing the initial PEG polymer concentration in hydrogel precursor solutions from 20 to 50 wt./wt.%. Glucose diffusion is a point of focus because glucose is a critical cell nutrient required by epithelial cells and, therefore, its diffusion rate through the hydrogel is directly relevant to ophthalmic applications. Maltose and maltotriose were examined in order to increase the diffusing solute size without significantly altering the chemistry of the solute.

How the observed diffusion coefficient of a solute within a polymer solution or network changes with polymer volume fraction has been the subject of many previous investigations and has resulted in a number of hindered diffusion models [8,9]. The applicability of two of these hindered diffusion models to our system is evaluated based on goodness-of-fit to experimental data. One model describes solute diffusion in polymer solutions and networks solely in terms of hydrodynamics, while the second model describes solute diffusion in polymer solutions and networks solely in terms of solute obstruction effects. These are described in the next section.

2. Background

2.1 Models for Hindered Diffusion in Hydrogels

A number of hindered diffusion models have been proposed to explain the observed decrease in solute diffusivity in the presence of polymer chains compared to that in pure solvent. Reviews

by Muhr and Blanshard and more recently by Amsden provide a detailed summary of various diffusion models presented in the literature [8,9]. In these hindered diffusion models, the observed diffusivity of a solute through a polymer gel, D_g, is compared to the diffusivity of a solute in pure solvent, D_0. A common feature of all hindered diffusion models is that the normalized diffusion coefficient, D_g/D_0, decreases with either increasing polymer volume fraction, φ, or increasing solute radius, r_s. Exactly how and why D_g/D_0 changes with respect to the polymer volume fraction, φ, and the solute radius, r_s, is a source of contention among various hindered diffusion models proposed in the literature.

Hindered solute diffusion through polymer solutions and networks has been variously modeled in terms of a reduction of free volume available to the solute, increased hydrodynamic drag experienced by the solute due to the presence of polymer chains, or polymer chains acting as physical obstructions to diffusion or effectively increasing the diffusion path length. The majority of the models for diffusion in polymer solutions and networks are derived based on one of these three phenomena or combinations thereof. The free volume theory of diffusion is based on the notion that solute diffusion in a pure liquid occurs by a solute jumping into voids within the liquid medium arising from molecular rearrangements. Models based on free volume theory have been less successful in the past, and the free volume theory of diffusion is a point of controversy for diffusion even in pure liquids [10,11]. For these reasons, we have chosen to focus on hindered diffusion models that are based on the more widely established hydrodynamic and obstruction phenomena to describe solute diffusion in polymer networks.

In this work, we present our diffusion data and compare it to two representative hindered diffusion models. The first model, originally developed by Cukier, is based on hydrodynamic considerations for diffusion in polymer networks and uses scaling relationships to relate the hydrodynamic screening length, κ^{-1}, to the volume fraction of polymer in the hydrogel, φ [12]. The second model was developed more recently by Amsden and is based on obstruction considerations [13]. The Amsden model also uses scaling relationships, but in this case the size of the spaces between polymer chains, ξ, is related to the volume fraction of polymer in the hydrogel, φ. The following provides a brief background on the two models.

Cukier Hydrodynamic Model—The origins of hydrodynamic models for hindered diffusion can be traced to papers from Debye/Beuche and a similar prior paper by Brinkman [14,15]. These papers describe the hydrodynamics of polymer solutions in terms of an effective medium model. Following the work of Debye/Beuche and Brinkman, Cukier proposed a model for hindered diffusion based solely on these hydrodynamic considerations [12]. Cukier's model uses a modified version of the Navier-Stokes equation to describe a polymer solution or network as a new “fluid” whose velocity, V(r), and pressure, P(r), satisfy equation 1. Equation 1 is the standard Navier-Stokes equation for fluid flow with an additional $\kappa^2 V(r)$ term. This term describes the hydrodynamic friction, which results from polymer chains being suspended in the solution, where κ^{-1} is the hydrodynamic screening length of this added friction. At a distance farther than this screening length, the hydrodynamic frictional force of a polymer chain will be effectively “screened out”. Scaling laws are used to determine how the screening length changes as a function of polymer concentration in different polymer concentration regimes.

$$\mu\nabla^2 V(r) - \kappa^2 V(r) - \nabla P(r) = F(r) \quad (1)$$

To determine the hydrodynamic friction experienced by a spherical solute of radius, r_s, the usual Stokes law derivation is performed using equation 1 rather than the standard Navier-Stokes equation. The friction experienced by a solute in the polymer network, f_g, divided by the friction experienced by the solute in pure solvent, f_0, is given in equation 2. Since only

hydrodynamic considerations are taken into account, the relationship between diffusion coefficients can be given as equation 3.

$$\frac{f_g}{f_0}=\exp(-\kappa r_s) \tag{2}$$

$$\frac{D_g}{D_0}=\exp(-\kappa r_s) \tag{3}$$

The Cukier model can then be expressed in terms of polymer volume fraction by relating the hydrodynamic screening length, κ^{-1}, to the polymer volume fraction, φ. It has been shown that there are at least three different scaling regimes with varying scaling relationships between the hydrodynamic screening length, κ^{-1}, and the polymer volume fraction, φ. In order from high polymer volume fraction to low polymer volume fraction, the scaling relationships are as follows: $\kappa^{-1}\sim\varphi^{-1}$, $\kappa^{-1}\sim\varphi^{-1/2}$, and $\kappa^{-1}\sim\varphi^{-3/4}$.[16] These scaling relationships can be used to rewrite equation 3 as equation 4 with a scaling exponent, *v*, and a proportionality constant, k. A detailed derivation of the Cukier hindered diffusion model can be found in Cukier's original paper [12].

$$\frac{D_g}{D_0}=\exp(-kr_s\varphi^{-v}) \tag{4}$$

Amsden Obstruction Model—Hindered diffusion models based on obstruction theories assume that the polymer chains in solution or within a network create fixed pores or openings within which the solute can diffuse. The polymer chains themselves act as obstructions to diffusion, effectively increasing the solute diffusion path length. Assumptions of the obstruction model are that the size, shape, location, and number of pores or openings within the polymer gel remain more or less fixed on the timescale of solute diffusion. A recent study by Zhang and Amsden showed that for polymer solutions, the polymer chains can be considered immobile over the timeframe of solute diffusion [17]. Therefore, it is reasonable to expect the same for polymer gels wherein polymer chain movement is more restricted.

The Amsden obstruction model has been developed in more recent years in comparison to the older Cukier hydrodynamic model but is based on work originally performed by Ogston et al. [13,18,19]. The Ogston model is a stochastic diffusion model wherein diffusion is considered to be the result of solute particles undergoing a series of statistically independent unit displacements. When a solute diffuses through a network of polymer chains, the solute can either undergo a unit step displacement or a collision with a polymer chain that results in no displacement. The probability of a solute encountering an opening in the network is expressed in terms of a distribution function, g(r), which describes the distribution of spaces between polymer chains. In the Ogston model, the distribution function and sizes of the spaces between polymer chains are determined by modeling the chains as a random array of rigid cylindrical fibers with finite radii equal to r_f [18]. Equation 5 shows the distribution function, g(r), for the distribution of spherical spaces in a random array of rigid fibers, where R is the mean radius of the distribution. Equation 6 shows that the normalized diffusion coefficient can then be expressed as the probability that a solute will encounter spaces large enough to diffuse through, where r* is the critical radius required for solute diffusion. Since this derivation models polymer chains as rigid cylinders, it cannot be expected to apply for flexible polymer hydrogels.

$$g(r) = \frac{\pi r}{2R^2} \exp\left(-\frac{\pi}{4}\left(\frac{r}{R}\right)^2\right) \tag{5}$$

$$\frac{D_g}{D_0} = \int_{r^*}^{\infty} g(r)\, dr \tag{6}$$

Although the Amsden model still uses the distribution of spaces derived by Ogston, the model is considered to be applicable to flexible chain systems because instead of using the size of the spaces between rigid cylindrical fibers, scaling relationships for flexible polymers are used to describe the size of the spaces between chains. The final form of the model derived by Amsden is shown in equation 7, where *v* is a scaling exponent, k is a proportionality constant, r_s is the size of the solute, and r_f is the effective radius of the polymer chains. Various versions of the Amsden model include additional parameters such as the interaction parameter, χ, and the characteristic ratio, C_n, to further refine the model for a given polymer system. Since these additional parameters end up getting absorbed into an undefined proportionality constant, k, we have presented the Amsden model in terms of this constant, which is used as a fitting parameter. A more detailed derivation of this model can be found in the original paper by Amsden [13].

$$\frac{D_g}{D_0} = \exp\left(-\pi\left(\frac{r_s + r_f}{k\varphi^{v} + 2r_f}\right)^2\right) \tag{7}$$

The value of the exponent, *v*, depends on the scaling relationship between the spacing between polymer chains, ξ, and the polymer volume fraction, φ. The proper scaling relationships were determined by Amsden by assuming that the polymer network is similar to a polymer solution of the same concentration. In this case, well-known scaling relationships for polymer solutions can be applied. These scaling relationships yield $\xi \sim \varphi^{-1}$ for the theta solvent regime, where polymer chains are considered to have ideal conformations and three-body monomer excluded volume interactions. For the good solvent regime, polymer chains have swollen chain conformations with two-body excluded volume effects and the scaling relationship $\xi \sim \varphi^{-3/4}$ applies. In between the good solvent regime and the theta solvent regime, a marginal solvent regime exists where polymer chains are considered to have ideal chain conformations and two-body interactions. In the marginal solvent regime $\xi \sim \varphi^{-1/2}$ applies [16,20,21].

For polyelectrolye networks such as those based on PAA, an alternative method to determine the proper scaling relationship was employed by Amsden [22]. For ionic networks with a low concentration of counterions present in solution, a force balance between osmotic swelling forces and elastic retractive forces of the polymer chains performed by Skouri et al. was used [23]. This yielded the scaling relationship, $\xi \sim \varphi^{-1/2}$, which is the same relationship as for the marginal solvent regime in polymer solutions. For ionic networks with a large concentration of counterions, Amsden reasoned that the electrostatic shielding from the high concentration of counterions would allow the polyelectrolyte network to be treated as a neutral polymer network. In this case, the scaling relationship for a polymer in a good solvent, $\xi \sim \varphi^{-3/4}$, applies.

The scaling relationships in the Cukier hydrodynamic model are associated with the hydrodynamic screening length, κ^{-1}, which is sometimes referred to as simply the dynamic screening length. Conversely, the scaling relationships in the Amsden obstruction model are associated with the average spacing between polymer chains, ξ, which is sometimes refered to

as the excluded volume or static screening length. Although the dynamic and static screening lengths represent physically different phenomena, both screening lengths are expected to follow the same scaling laws [16,24]. This means that the Cukier and Amsden models use the same scaling exponents to relate screening lengths to the polymer volume fraction. In the Cukier model, only hydrodynamic effects are included in the scaling relationships, while in the Amsden model, only obstruction effects are present in the scaling relationships.

3. Materials and Methods

3.1 Chemicals

2-Hydroxy-2-methyl-propiophenone, acrylic acid, acryloyl chloride, glucose, maltose, maltotriose, poly(ethylene glycol) (PEG) (M_n≈4600 Da), and triethylene glycol dimethacrylate, were purchased from Aldrich Chemical Co. (Milwaukee, WI) and used as received. Anhydrous tetrahydrofuran (THF) was purchased from Fisher Scientific (Pittsburg, PA). Phosphate buffered saline pH 7.4 (PBS pH 7.4) was purchased from Invitrogen (Carlsbad, CA).

3.2 Hydrogel Preparation

IPN hydrogels consisting of a PEG network interpenetrated with a PAA network were prepared as described previously [4]. Briefly, PEG/PAA IPN hydrogels were prepared with a two-step, sequential, UV-initiated free radical polymerization. Poly(ethylene glycol)-diol terminated macromonomer, M_n≈4600 Da, was dissolved in anhydrous THF at 50°C, a molar excess of acryloyl chloride was added, and the reaction mixture was then allowed to react for 5 hours under a nitrogen atmosphere. The poly(ethylene glycol)-diacrylate (PEG-DA) product was then purified by recrystallization twice in THF at 4°C. To create a single network PEG hydrogel, PEG-DA macromonomer (M_n≈4600) was dissolved in deionized water at 20, 30, 40, and 50 wt./wt.% concentrations. The photoinitiator, 2-hydroxy-2-methyl-propiophenone, was then added to the PEG-DA solution at 1 wt.% with respect to the macromonomer. Finally, the PEG-DA macromonomer precursor solution was injected between two glass slides separated by a 250 μm spacer and exposed to a UV light source, 365 nm at 10mW/cm^2, for 5 min. (UV chamber model ELC-500, Electro-lite Corporation, Danbury, CT). Upon exposure to UV light, the acrylate groups reacted to create an end-linked PEG network.

To create a PEG/PAA IPN hydrogel, the PEG single network hydrogel was soaked in a large excess of a 50 v.% (7.3 M) acrylic acid monomer solution with 1% v./v. 2-hydroxy-2-methyl-propiophenone photoinitiator (0.45 mol.% with respect to acrylic acid monomer) and 1% v./v. triethylene glycol dimethacrylate crosslinker (0.26 mol.% with respect to acrylic acid monomer). The PEG hydrogel was allowed to soak in the acrylic acid solution overnight and was then placed back between glass slides separated by spacers and exposed to UV light for 5 min. After the second polymerization step, the PEG/PAA IPN hydrogel was washed in phosphate buffered saline (PBS) (pH 7.4, ionic strength 0.15 M) until the pH remained constant. PBS pH 7.4 is used to mimic physiological pH and ionic strength conditions.

3.3 Hydrogel Equilibrium Volume Fraction Determination

To determine the mass fraction of PEG, PAA, and total polymer in the equilibrium swollen hydrogels, 12 mm discs were cut out after the first polymerization step. The swollen masses of these discs were recorded before and after each polymerization step and after equilibrium swelling in PBS buffer at pH 7.4. After each polymerization step, the weight of hydrogel discs after drying overnight in a vacuum desiccator was also recorded to obtain the polymer mass in the hydrogels. The mass fractions of PEG, PAA, and total polymer were then converted into volume fractions using 0.92 cm^3/g as the specific volume of PEG and 0.82 cm^3/g as the specific volume of PAA [25]. There were negligible deviations in equilibrium volume fraction between

samples of the same composition. Converting mass fractions to volume fractions was seen as a more accurate method than attempting to measure volumes of very small dried hydrogel samples directly.

3.4 Diffusion Coefficient Determination

Diffusion coefficients of glucose, maltose, and maltotriose were obtained via solute diffusion through thin hydrogel discs (diameter=12 mm, thickness=0.68-0.77 mm). The hydrogels are considered to be thin in relation to their radial dimensions such that a one-dimensional diffusion model is considered accurate. Hydrogels of roughly the same thickness were used. By so doing, any possible boundary layer effects present will affect each sample to the same degree and the relative differences between diffusion coefficients obtained for different sample compositions should be valid.

To perform the diffusion coefficient measurements, the hydrogel discs were placed in modified blind well chambers (model BW200S, NeuroProbe, Gaithersburg, Md.). The blind well chambers consist of an upper (receptor cell) and a lower (donor cell) chamber, each 200 μL in volume. Figure 1 shows a diagram of the chambers used for diffusion studies. The chambers have a 4.7 mm diameter opening, yielding a 17.35 mm^2 area available for solute diffusion through Sample aliquots hydrogel samples. One face of the hydrogel is kept at a constant solute concentration by modifying the lower chamber to allow a continuous flow of 75 μL/min. of a 56 mM solute concentration in PBS buffer pH 7.4. This concentration is considered to be high relative to the concentration on the opposite side of the hydrogel face during data collection, yet negligible compared to the total solute concentration in the PBS buffer such that there is a negligible osmotic pressure difference between the two faces of the hydrogel. Any possible leakage between upper and lower chambers could easily be observed by a change in solution volume in the upper receptor cell. The upper receptor chamber was stirred with a magnetic stir bar (volume=0.018 cm^3) to maintain a uniform solute concentration. The volume of the stir bar was taken into account when using the volume of the upper receptor chamber to calculate the diffusion coefficient. The concentration of solute in the upper receptor chamber was measured with 0.3 μL sample volume per measurement at thirty-minute intervals until six data points were obtained. The small volume for sample measurement is considered negligible compared to the total volume of the receptor chamber. The data points collected yielded a linear relationship between concentration and time during the timeframe of data collection. Figure 2 shows a typical linear relationship observed between solute concentration and time. The slope of a linear fit to this data was then used to determine the diffusion coefficient, as described below.

To determine the diffusion coefficient, the one-dimensional diffusion equation (Fick's second law) is solved in Cartesian coordinates with the initial condition $C(t=0)=0$ and boundary conditions $C(x=0)=C_1=56$ mM and $C(x=L)=C_2\approx 0$, where C_1 is the concentration of solute in the lower (donor) chamber and C_2 is the concentration of solute in the upper receptor chamber. Although C_2 obviously increases with time, C_1 is always significantly higher than C_2 when data points are collected, such that the value of C_2 is approximated as zero. This assumption is justified by the fact that the solute concentration vs. time plots (Figure 2) are linear over the range of data point collection. Once the value of C2 approaches that of C1, this assumption breaks down and the concentration vs. time plots will no longer be linear. The diffusion coefficient, D_g, of the solute in the hydrogel can be calculated using the slope of the linear portion of the concentration vs. time plot and the steady-state solution to the one-dimensional diffusion equation given as equation 8, where Q_t is the total amount of solute that has passed through the hydrogel thickness, L, at time t [26]. Diffusion measurements for each hydrogel composition and solute pair were repeated four times to obtain replicate data. The diffusion

coefficients for all four trials were averaged and are reported as averages with standard deviations as the error bars.

$$Q_t = \frac{D_g C_1}{L}\left(t - \frac{L^2}{6D_g}\right) \tag{8}$$

3.5 Solute Concentration Measurement

Concentrations of glucose, maltose, and maltotriose were measured with a FreeStyle over-the-counter blood glucose meter manufactured by Abbott (Abbott Park, Il). The FreeStyle blood glucose meter uses an electrochemical method to determine the concentration of glucose in a sample. Briefly, glucose is oxidized to gluconolactone via glucose dehydrogenase enzymes embedded in test strips. The device uses a coulometric method for determining glucose concentrations, meaning that all of the glucose in the sample is reacted and the total charge generated during this reaction is used to determine the glucose concentration. The FreeStyle glucose meter is able to measure glucose concentrations ranging from 1.1 to 27.8 mM (+/- 0.1-0.8 mM) with sample volumes as small as 0.3 μL [27]. The glucose dehydrogenase enzyme in the test strips is also able to react with disaccharides and trisaccharides with α(1→4) linkages. Therefore, the FreeStyle glucose meter is also capable of reliably determining the concentrations of maltose and maltotriose in addition to glucose, as demonstrated in calibration curves for each solute. Figure 3 shows the calibration curves that demonstrate the ability of the FreeStyle glucose meter to measure glucose, maltose, and maltotriose concentrations.

3.6. Partition Coefficient Determination

Partition coefficients for each solute were determined by adding a known concentration of solute to a known volume of hydrogel and buffer. The concentrations of the solute in solution were measured after the solute was allowed to reach an equilibrium between the hydrogel and the solution phases (one week). Data were collected in triplicate for each hydrogel composition and solute pair. Equation 9 was derived from a mass balance between the hydrogel and solution phases and was used to calculate partition coefficients. Here C_0 is the initial solute concentration in solution, C_e is the solute concentration in solution at equilibrium, V_s is the volume of the solution, and V_g is the volume of the hydrogel. In all cases, the partition coefficients were determined to be 1.0±0.3. Since all of the partition coefficients were found to be near unity within experimental scatter, the partition coefficients were taken to be precisely unity. This implies that the observed permeability (D_g*K_d) is equivalent to the observed diffusivity (D_g).

$$K_d = \frac{V_s (C_0 - C_e)}{V_g C_e} \tag{9}$$

3.7. Fitting to Hindered Diffusion Models

For both the Cukier and Amsden models, the decrease in diffusion rate of a solute within a hydrogel compared to that in pure solvent is evaluated based on two key parameters: the equilibrium volume fraction of polymer, φ, and the hydrodynamic radius of the solute, r_s. To evaluate the effect of the polymer volume fraction on the diffusion rate of solutes in PEG/PAA IPN hydrogels, the equilibrium polymer fraction was varied systematically by varying the initial weight percent of PEG in hydrogel precursor solutions from 20 to 50 wt./wt.%. Precursor solutions with a higher weight percent PEG could not be prepared due to poor solubility of the polymer, while lower weight percent precursor solutions did not completely gel upon UV exposure, probably due to a high rate of intrachain cyclization. For these reasons, hydrogels

with significantly higher or lower volume fraction of polymer could not be obtained without changing additional parameters in the system. In this study, we chose to vary only one parameter in the PEG/PAA IPN hydrogel system in order to avoid adding additional complications. To evaluate the effect of solute radius on the solute diffusion rate observed in PEG/PAA IPN hydrogels, diffusion experiments were carried out for glucose, a monosaccharide; maltose, a disaccharide; and maltotriose, a trisaccharide. This series provides a controlled method to evaluate the effect of increased solute size while maintaining a similar solute chemistry and allowing the same detection method to be used for each solute.

Nonlinear curve fitting of hindered diffusion models to experimental diffusion data was performed via a Levenburg-Marquardt nonlinear regression algorithm using OriginLab software (OriginLab, Northampton, MA). The validity of the hindered diffusion model was assessed in terms of the values of the fitting parameters returned as well as the values of the adjusted coefficients of determination, R^2. To assess the ability of the hydrodynamic-based Cukier model and the obstruction-based Amsden model to predict hindered diffusion coefficients in PEG/PAA IPN hydrogels, the models were fit to both normalized diffusion coefficient, $D_g/D_{0,}$ versus polymer volume fraction, φ, data and normalized diffusion coefficient, D_g/D_0, versus solute radius, r_s, data. In this way, the ability of the model to predict both the influence of the polymer volume fraction in the hydrogel and the solute radius may be evaluated.

Each of the models examined in this work contains the radius of the solute diffusing through the hydrogel as a key parameter. The hydrodynamic radii of glucose, maltose, and maltotriose were obtained using the Stokes-Einstein relationship (equation 10) for equivalent spheres with the same diffusion coefficients as reported for the solutes in pure solvent. In the Stokes-Einstein relationship, the diffusion coefficient is expressed in terms of the thermal energy of the system, k_BT, and the hydrodynamic drag, γ, acting on a sphere of radius, $r_{s,}$ which is expressed in terms of solvent viscosity, η. The diffusion coefficients for each solute in water at 25°C, D_0, were obtained from values reported in the literature [28]. The diffusion coefficient reported for raffinose, another trisaccharide, was used in place of maltotriose.

$$D_0=\frac{k_BT}{\gamma}=\frac{k_BT}{6\pi\eta r_s} \tag{10}$$

In addition to the radius of the diffusing solute, the Amsden model also contains the radius of the polymer chains in the network, r_f, as a parameter that must be either estimated or used as a fitting parameter. To maintain the same number of fitting parameters for each model, we have estimated the radius of the polymer chains by weight-averaging values obtained for both PAA and PEG based on the relative proportions of PAA and PEG in the IPN hydrogels. According to Tayler et al. and references therein, PAA can be modeled as a cylindrical worm-like chain with radius 3.0 Å, so this value was taken as the chain radius for PAA [29]. For the chain radius of PEG, ChemDraw software (CambridgeSoft, Cambridge, MA) was used to determine the radius of a Kuhn length segment of PEG, which consists of two monomer units. The radius of the PEG segment was determined to be 2.4 Å. The chain radii for the two polymers were weight averaged based on the volumetric ratios of PAA:PEG in the IPN hydrogels. Although the ratio of PAA to PEG in the IPN hydrogels varied between samples, using either the highest ratio of PAA:PEG (9.167:1) or the lowest ratio of PAA:PEG (5.117:1) yielded the same weighted average chain radius within 0.1 Å. To account for the hydration sheath surrounding the polymer chains, the diameter of one water molecule, taken as 2.8 Å, was added to the weighted average polymer chain radius, yielding a chain radius of 5.7 Å. Since the chain radii for both polymers were determined to be very close, the obvious simplification of weight averaging the two radii is not expected to have a large influence on the model.

4. Results and Discussion

4.1. Hydrogel Equilibrium Swelling

The equilibrium volume fraction of polymer in PEG/PAA IPN hydrogels swollen in PBS buffer at pH 7.4 was varied by changing the PEG macromonomer concentration in the hydrogel precursor solutions. Hydrogels with PEG macromonomer $M_n \approx 4600$ g/mol were prepared with varying initial macromonomer concentrations ranging from 20 to 50 wt./wt.%. Decreasing the initial concentration of PEG decreased the overall equilibrium volume fraction of polymer in PEG/PAA IPN hydrogels from a volume fraction of 0.174 to 0.075. Decreasing the initial concentration of PEG also had the effect of changing the volumetric ratio of PAA:PEG in the final IPN hydrogel from 5.177:1 to 9.167:1. The equilibrium volume fractions of PEG, PAA, and total polymer volume fractions of all hydrogels used in this study are summarized in Table 1.

4.2. Fitting To Hindered Diffusion Models

A key parameter in the Cukier model is the relationship between the hydrodynamic screening length, κ^{-1}, and the polymer volume fraction, φ. It has been proposed that the hydrodynamic screening length has at least three different scaling regimes where there are different scaling exponents relating this screening length to the polymer volume fraction [16]. We chose to fit our data to versions of the Cukier model with three of the proposed scaling relationships to determine which scaling relationship provides the most appropriate fit. A plot of D_g/D_0 vs. φ data fit to the Cukier model with the hydrodynamic screening length scaling as either $\kappa^{-1} \sim \varphi^{-1}$, $\kappa^{-1} \sim \varphi^{-3/4}$, or $\kappa^{-1} \sim \varphi^{-1/2}$ is shown in Figure 4a. The Amsden obstruction model also has several versions with varying scaling relationships between parameters. In this case, how the spacing between polymer chains or the static screening length, ξ, scales with the polymer volume fraction, φ, is the key parameter. A plot of D_g/D_0 vs. φ data fit to the Amsden model with the static screening length scaling as either as either $\xi \sim \varphi^{-1}$, $\xi \sim \varphi^{-3/4}$, or $\xi \sim \varphi^{-1/2}$ is shown in Figure 4b.

Figure 5 shows a comparison plot of the best fits for the Cukier model ($\kappa^{-1} \sim \varphi^{-1/2}$) and the Amsden model ($\xi \sim \varphi^{-1}$) to both D_g/D_0 vs. φ and D_g/D_0 vs. r_s data. Figure 5a shows a comparison between the two models for D_g/D_0 vs. φ data, while Figure 5b shows a comparison between the two models for D_g/D_0 vs. r_s data. Since the D_g/D_0 vs. r_s data are not affected by the different scaling relationships employed, only the results of the best scaling relationships (obtained from fits to D_g/D_0 vs. φ data) are shown.

Table 2 contains a summary of the fitting parameters obtained for each model and the R^2 values for each fit to the data. The standard errors for the proportionality constants, k, obtained from model fits to the data have been included. If the proportionality constant, k, is a meaningful parameter for a given polymer/solute combination, then the values returned for this fitting constant should remain roughly the same for fitting the model to either D_g/D_0 vs. φ or D_g/D_0 vs. r_s data.

4.3. Analysis of Modeling Fitting

PEG/PAA IPN hydrogels are distinguished from most other hydrogels in that they have both a low volume fraction of polymer (≤ 0.2) and high mechanical st rength (initial modulus $E_i \approx 2$-10 MPa) [4,5]. PEG and PAA chains in solution have been previously shown to form interpolymer hydrogen bonding complexes at low pH [30-32]. At high pH, the hydrogen bonding complex between PEG and PAA reversibly disassociates as the carboxylic acid groups along the PAA chains become deprotonated. Acrylic acid has also been shown to template polymerize along PEG chains in solution when polymerized at low pH [33]. It is currently unclear what effect hydrogen bonding during formation of PEG/PAA IPNs at low pH has on

the structure when the hydrogel is swollen in buffer pH 7.4, a condition in which PAA is fully deprotonated. Given the likely hydrogen bonding interaction between these two polymers and the fact that PEG/PAA IPNs exhibit a dramatic enhancement in mechanical properties compared to most single network hydrogels, the structure of these IPN hydrogels on the molecular level could be expected to be more complex than most single network hydrogels widely used in solute diffusion studies. One of the objectives of this work to determine if small molecule diffusion through PEG/PAA IPN hydrogels can be accurately fit by hindered diffusion models previously described, and if so, which models provide the best fit to the data.

For the Cukier hydrodynamic model, three different versions were fit to the data with the hydrodynamic screening length scaling with the polymer volume fraction as either $\kappa^{-1}\sim\varphi^{-1}$, $\kappa^{-1}\sim\varphi^{-3/4}$, or $\kappa^{-1}\sim\varphi^{-1/2}$. From analysis of the Cukier model fits to experimental data in Figure 4 as well as the R^2 values and differences in k values reported in Table 2, it is clear that the hydrodynamic screening length scaling as $\kappa^{-1}\sim\varphi^{-1/2}$ provides a much better fit to the data than the other scaling relationships. For $\kappa^{-1}\sim\varphi^{-1/2}$ scaling, R^2=0.71 for fits to D_g/D_0 vs. φ data and R^2=0.66 for fits to D_g/D_0 vs. r_s data. As discussed in the original paper by Cukier, previous studies on solute sedimentation and diffusion in polymer solutions have shown that normalized diffusion coefficient vs. polymer volume fraction, D_g/D_0 vs. φ, data can be accurately fit to a stretched exponential of the polymer volume fraction to the one-half power [12,34]. The Cukier model has this form if $\kappa^{-1}\sim\varphi^{-1/2}$ scaling is employed. Thus, our data are consistent with previous results that show this form of the Cukier model best describes hindered diffusion in polymer solutions and networks, although the fit is only moderately successful.

In a similar approach, three different versions of the Amsden model were fit to our data. In this case, the scaling relationships used to relate static screening length to the polymer volume fraction are $\xi\sim\varphi^{-1}$, $\xi\sim\varphi^{-3/4}$, and $\xi\sim\varphi^{-1/2}$. The data presented in Figure 4 and Table 2 indicate that calculations of the Amsden model with the scaling relationships $\xi\sim\varphi^{-1}$ and $\xi\sim\varphi^{-3/4}$ fit very well to D_g/D_0 vs. φ data, with R^2=0.98 and R^2=0.96, respectively. Fitting to the scaling relationship $\xi\sim\varphi^{-1/2}$ provides a poorer fit to the data with an R^2=0.78. This fit is notably worse than the fits obtained with either $\xi\sim\varphi^{-1}$ or $\xi\sim\varphi^{-3/4}$ scaling, but is still better than the best fit obtained with the Cukier model. The Amsden model was also able to fit D_g/D_0 vs. r_s data better than the Cukier model with R^2=0.89 as opposed to R^2=0.66 for the Cukier model. For all of the Amsden model fits, the proportionality constants or k values returned for fits to both D_g/D_0 vs. φ and D_g/D_0 vs. r_s data fall within the standard errors returned by the fitting algorithm. This means that the values for the proportionality constants are consistent whether or not the model is fitting changes in volume fraction or solute radius. Figure 5 shows a comparison of the best fits obtained from both the Cukier and Amsden models for both polymer volume fraction and solute radius dependence. The data show that the Amsden obstruction model, regardless of the scaling relationship employed, provides an improved prediction of hindered diffusion coefficients compared to the Cukier hydrodynamic model.

It might be expected that hindered diffusion in PEG/PAA IPNs follows that predicted by models for the single components of the IPN. A polyelectrolyte such as PAA with sufficient charge screening from counter ions, as is the case in 0.15M PBS, can be treated as a polymer in a good solvent with $\xi\sim\varphi^{-3/4}$ scaling [22]. For the PEG network, a study by Cheng et al. on solute diffusion in higher molecular weight PEG solutions yielded scaling exponent values between 0.66 and 0.97 depending on the type of solute used [35]. These results are consistent with our data that show the Amsden model provides a good fit with scaling exponents of either $\xi\sim\varphi^{-3/4}$ or $\xi\sim\varphi^{-1}$. An inconsistency present in these results is that the scaling exponent $\xi\sim\varphi^{-3/4}$ is derived from an assumption that the polymer chains are behaving as in a good solvent while $\xi\sim\varphi^{-1}$ scaling is derived from an assumption that the polymer chains are behaving as in a theta solvent. If both of these scaling exponents are able to fit the data, then little information can be obtained about the possible chain conformations in PEG/PAA IPN hydrogels. The

Amsden model is in fact sensitive to which scaling exponent is employed, but only at much lower volume fractions of polymer than those probed in this study. Unfortunately, it is difficult to obtain PEG/PAA IPN hydrogels with such low volume fractions of polymer without significantly changing a number of parameters in the system. Given this limitation in our system, it is difficult to infer information about chain conformation in PEG/PAA IPN hydrogels using this model.

5. Conclusions

We have fit our diffusion data to both a hydrodynamic model originally proposed by Cukier and to an obstruction model developed more recently by Amsden. Both the Cukier and Amsden models rely on scaling theories to predict diffusion coefficients in polymer solutions and networks. For the Cukier hydrodynamic model, the hydrodynamic screening length, κ^{-1}, scaling as $\kappa^{-1}\sim\varphi^{-1/2}$ provides the best fit to our data, although the fit is only moderate. This is consistent with previous findings that show that the Cukier model with $\kappa^{-1/2}\sim\varphi^{-1/2}$ scaling provides a better fit than other scaling relationships used for this model. The Amsden model provides a very close fit to our experimental data; however, care must be taken in extracting information regarding the proper scaling relationships for PEG/PAA IPN hydrogels because the model is not extremely sensitive to the scaling relationship employed over the range of polymer volume fractions explored in this work. Since it is difficult to obtain PEG/PAA IPN hydrogels with very low volume fractions of polymer, it is difficult to determine the proper scaling relationship for this system with this model. Despite this limitation, the Amsden obstruction model is able to provide a better prediction of both the polymer volume fraction dependence and solute radius dependence of saccharide diffusion through PEG/PAA IPN hydrogels than the Cukier hydrodynamic model. This demonstrates that despite the potentially more involved molecular level structures of PEG/PAA IPN hydrogels, a coarse-grained model based solely on obstruction effects is able to accurately fit both the polymer volume fraction and solute radius dependence of normalized solute diffusion coefficients observed in these IPN hydrogels.

On-going and planned small angle x-ray (SAXS) and small angle neutron scattering (SANS) measurements will help to determine the average size of the spaces between polymer chains in PEG/PAA IPN hydrogels and how the sizes of these spaces scale with the equilibrium volume fraction of polymer. Since it has been shown that the hydrodynamic screening length and the static screening length scale similarly with the polymer volume fraction, the scaling relationship obtained from scattering measurements should apply to both the Cukier and the Amsden hindered diffusion models [16]. Once the proper scaling relationship for this system is established by experimental scattering methods, the validity and accuracy of the hindered diffusion models presented in this work can be more thoroughly assessed.

Acknowledgments

The authors wish to thank the National Institutes of Health (NIH) grant R01 EY016987-01A1 and the Singapore Eye Research Institute (SERI) for funding. We also wish to thank Professor Christopher Ta, Department of Ophthalmology, Stanford University, for useful discussions.

References

1. Hoare TR, Kohane DS. Polymer 2008;49(8):1993–2007.
2. Kopecek J, Jiyuan Y. Polymer International 2007;56(9):1078–1098.
3. Gong JP, Katsuyama Y, Kurokawa T, Osada Y. Advanced Materials 2003;15(14):1155–1158.
4. Myung D, Koh WU, Ko JM, Hu Y, Carrasco M, Noolandi J, Ta CN, Frank CW. Polymer 2007;48(18): 5376–5387.

5. Myung D, Waters D, Wiseman M, Duhamel PE, Noolandi J, Ta CN, Frank CW. Polymers for Advanced Technologies 2008;19(6):647–657. [PubMed: 19763189]
6. Myung D, Koh W, Bakri A, Zhang F, Marshall A, Ko JM, Noolandi J, Carrasco M, Cochran JR, Frank CW, Ta CN. Biomedical Microdevices 2007;9(6):911–922. [PubMed: 17237989]
7. Myung D, Farooqui N, Waters D, Schaber S, Koh W, Carrasco M, Noolandi J, Frank CW, Ta CN. Current Eye Research 2008;33(1):29–43. [PubMed: 18214741]
8. Amsden B. Macromolecules 1998;31(23):8382–8395.
9. Muhr AH, Blanshard JMV. Polymer 1982;23(7):1012–1026.
10. Tyrrell, HJV.; Harris, KR. Diffusion in Liquids: A Theoretical and Experimental Study. Butterworths; London: 1984.
11. Amsden B. Polymer 2002;43(5):1623–1630.
12. Cukier RI. Macromolecules 1984;17(2):252–255.
13. Amsden B. Macromolecules 1999;32(3):874–879.
14. Debye P, Bueche AM. Journal of Chemical Physics 1948;16(6):573–579.
15. Brinkman HC. Applied Scientific Research 1947;A 1(1):27–34.
16. Uematsu T, Svanberg C, Jacobsson P. MACROMOLECULES 2005;38(14):6227–6230.
17. Zhang Y, Amsden BG. Macromolecules 2006;39(3):1073–1078.
18. Ogston AG. Transactions of the Faraday Society 1958;54(11):1754–1757.
19. Ogston AG, Preston BN, Wells JD, Ogston AG, Preston BN, Snowden JM, Wells JD. Proceedings of the Royal Society of London Series A-Mathematical Physical and Engineering Sciences 1973;333 (1594):297–316.
20. Schaefer DW. Polymer 1984;25(3):387–394.
21. DeGennes, PG. Scaling Concepts in Polymer Physics. Cornell University Press; Ithaca, NY: 1979.
22. Amsden B. Macromolecules 2001;34(5):1430–1435.
23. Skouri R, Schosseler F, Munch JP, Candau SJ. Macromolecules 1995;28(1):197–210.
24. DeGennes PG. Macromolecules 1976;9(4):594–598.
25. Welsh, WJ. Physical Properties of Polymers Handbook. AIP Press; Woodbury, NY: 1996.
26. Crank, J. The Mathematics of Diffusion. 2nd Edition. Oxford University Press; New York: 2001.
27. Feldman B, McGarraugh G, Heller A, Bohannon N, Skyler J, DeLeeuw E, Clarke D. Diabetes Technology & Therapeutics 2000;2(2):221–229. [PubMed: 11469262]
28. Longsworth LG. Journal of the American Chemical Society 1953;75(22):5705–5709.
29. Taylor TJ, Stivala SS. Journal of Polymer Science, Part B: Polymer Physics 2003;41(12):1263–1272.
30. Oyama HT, Tang WT, Frank CW. Macromolecules 1987;20(3):474–480.
31. Yu XH, Tanaka A, Tanaka K, Tanaka T. Journal of Chemical Physics 1992;97(10):7805–7808.
32. Adachi H, Nishi S, Kotaka T. Polymer Journal 1982;14(12):985–992.
33. Polowinski S. Progress in Polymer Science (Oxford) 2002;27(3):537–577.
34. Laurent TC, Bjork I, Persson H, Pietruszkiewicz A. Biochimica Et Biophysica Acta 1963;78(2):351–359. [PubMed: 14099644]
35. Cheng Y, Prud'homme RK, Thomas JL. Macromolecules 2002;35(21):8111–8121.

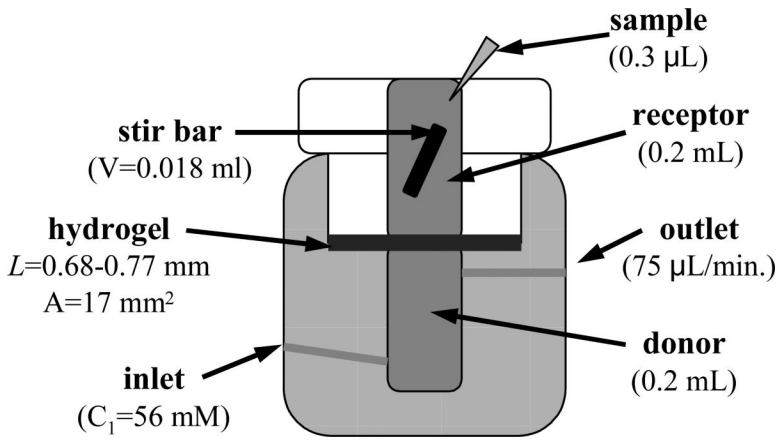

Fig. 1.

Diagram of modified blind well chambers used for diffusion measurements. A hydrogel sample separates the lower donor chamber from the upper receptor chamber. A 75 μL/min flow of solute through the bottom chamber maintains a constant 56 mM solute concentration at the bottom face of the hydrogel. Sample aliquots 0.3 μL in volume are taken from the receptor chamber to obtain a solute concentration versus time plot.

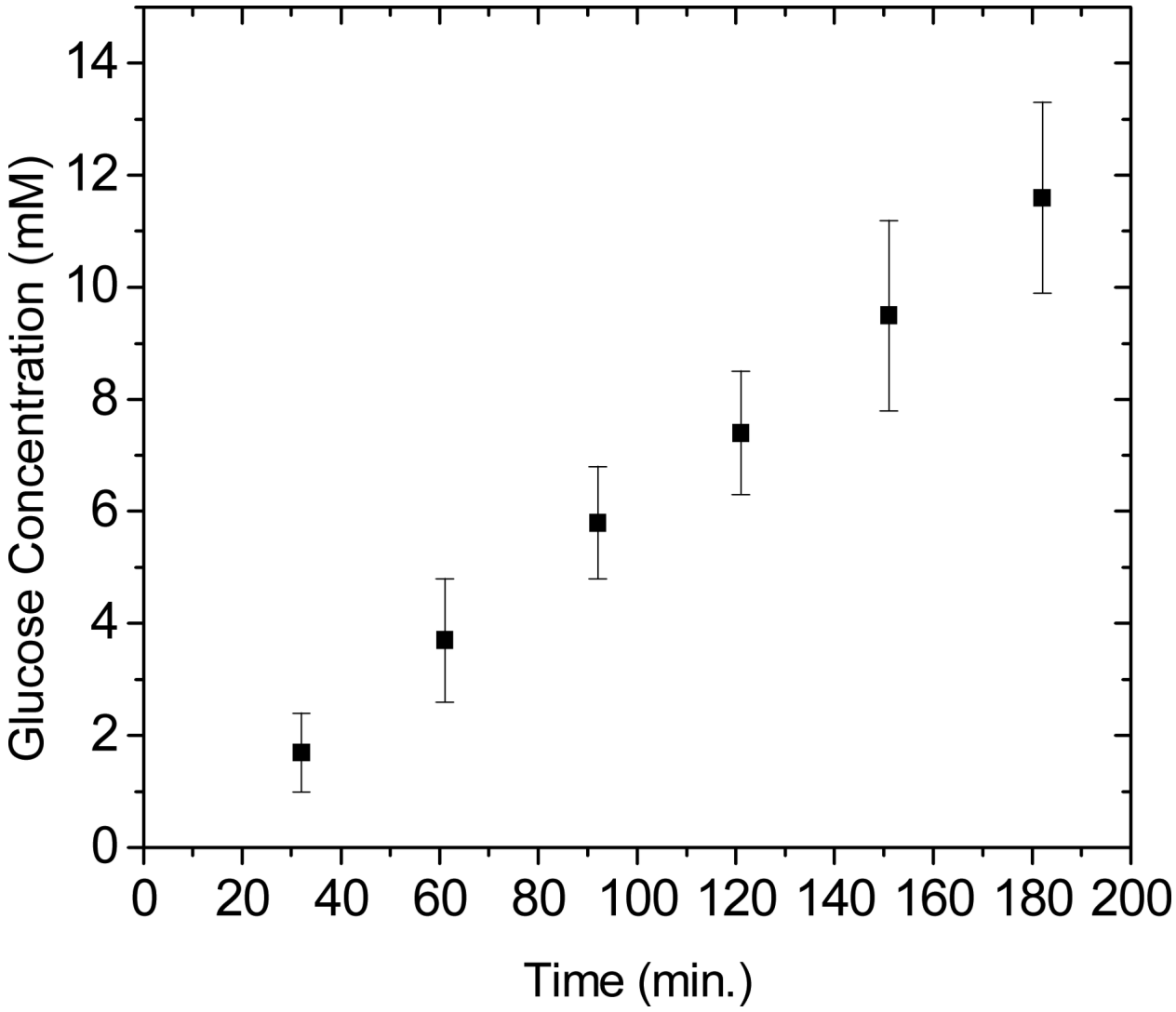

Fig. 2.

A representative concentration versus time curve for glucose diffusing through PEG M_n≈4600 Da, 50 wt.% initial PEG content/PAA IPN hydrogel. A linear relationship between concentration and time is observed over the time period of data collection.

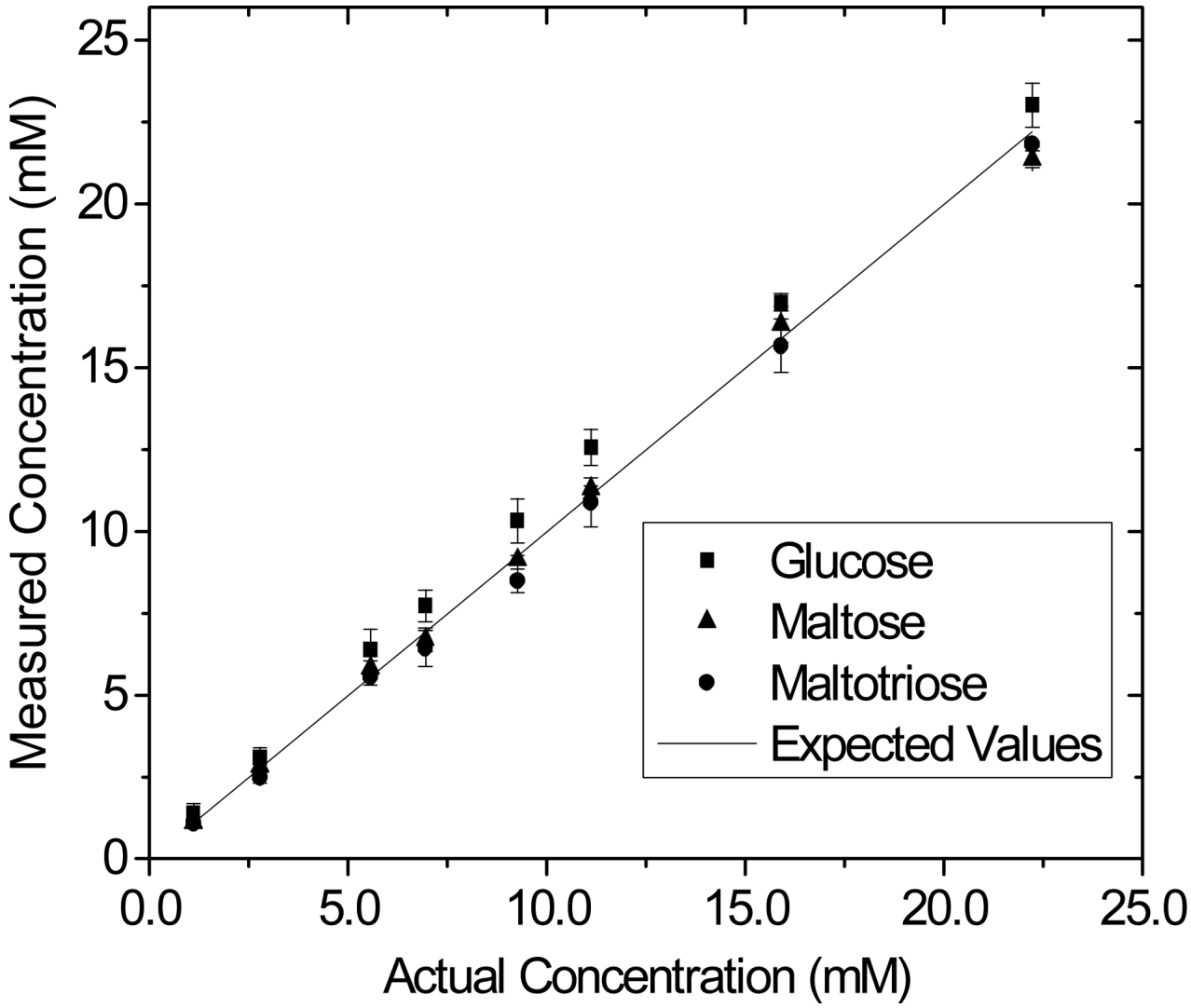

Fig. 3.
Calibration curve showing the solute concentrations measured by the Freestyle glucose meter versus the actual solute concentrations. The Freestyle glucose meter is able to accurately measure the concentration of glucose, maltose, and maltotriose.

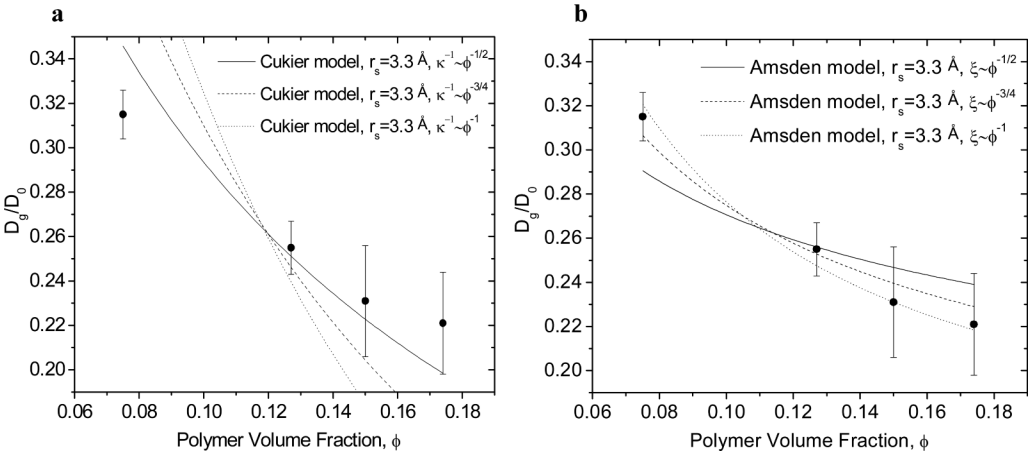

Fig. 4.

(a) Normalized diffusion coefficient, D_g/D_0, versus polymer volume fraction, φ, fit to the Cukier hydrodynamic model. Varying scaling exponents relating the hydrodynamic screening length, κ^{-1}, to the polymer volume fraction, φ, were employed. (b) Normalized diffusion coefficient, D_g/D_0, versus polymer volume fraction, φ, fit to the Amsden obstruction model. Varying scaling exponents relating the spacing between polymer chains, ξ, to the polymer volume fraction were employed. All data points are average values with error bars representing one standard deviation in experimental data.

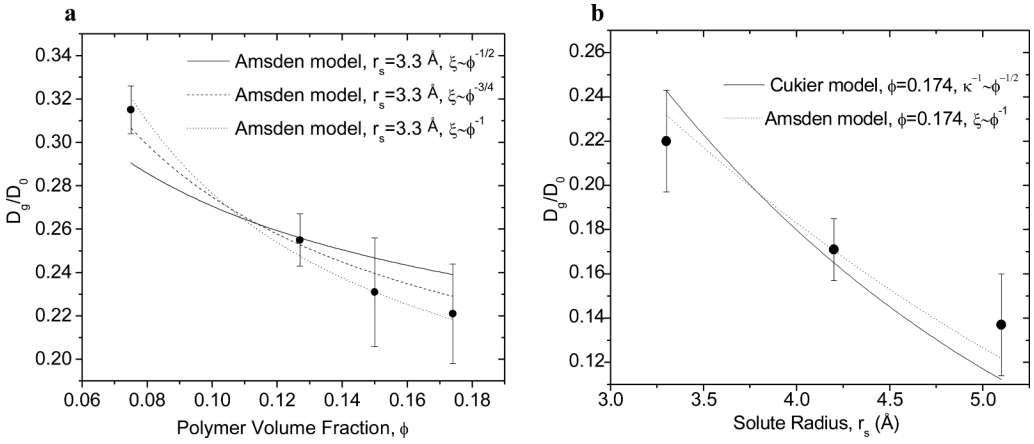

Fig. 5.

(a) Comparison between the best fit obtained with the Amsden model and the best fit obtained with the Cukier model for normalized diffusion coefficient, D_g/D_0, versus polymer volume fraction, φ. (b) Comparison between the best fit obtained with the Amsden model and the best fit obtained with the Cukier model for normalized diffusion coefficient, D_g/D_0, versus solute radius, r_s, data. In each plot error bars represent one standard deviation.

Table 1

Volume fractions of PEG, PAA, and total polymer content were obtained by taking the mass of hydrogels in the equilibrium swollen and dried states and converting to volume using v_{sp}=0.92 cm^3/g for PEG and v_{sp}=0.82 cm^3/g for PAA [25].

Hydrogel Composition	Vol. frac. PAA	Vol. frac. PEG	Vol. Ratio PAA:PEG	Mol. Ratio AA/EO	Vol. Frac. Polymer
PEG4.6k-50%/PAA	0.146	0.028	5.177	3.550	0.174
PEG4.6k-40%/PAA	0.128	0.021	6.004	4.117	0.150
PEG4.6k-30%/PAA	0.109	0.018	6.118	4.195	0.127
PEG4.6k-20%/PAA	0.068	0.007	9.167	6.285	0.075

Table 2

Summary of adjusted coefficients of determination, R^2, and proportionality constants, k, used as fitting parameters for fits to the Cukier hydrodynamic and Amsden obstruction models.

Volume Fraction Dependence				Solute Radius Dependence			
Model	**Scaling**	**k**	**R^2**	**Model**	**Scaling**	**k**	**R^2**
Amsden	1.0	0.27±0.01	0.98	Amsden	1.0	0.31±0.03	0.89
Amsden	0.75	0.47±0.02	0.96	Amsden	0.75	0.48±0.05	0.89
Amsden	0.5	0.81±0.07	0.78	Amsden	0.5	0.75±0.07	0.89
Cukier	0.5	1.18±0.04	0.71	Cukier	0.5	1.03±0.05	0.66
Cukier	0.75	2.00±0.16	-0.67	Cukier	0.75	1.59±0.08	0.66
Cukier	1.0	3.41±0.45	-3.12	Cukier	1.0	2.47±0.12	0.66